International Journal of Automotive Technology, Vol. 17, No. 2, pp. 213–223 (2016)
DOI 10.1007/s12239–016–0021–1

Copyright © 2016 KSAE/ 089–03
pISSN 1229–9138/ eISSN 1976–3832

ANALYSIS OF AUTOMOTIVE DISC BRAKE SQUEAL CONSIDERING DAMPING AND DESIGN MODIFICATIONS FOR PADS AND A DISC

C. KIM* and K. ZHOU

Department of Mechanical Engineering, Kyungpook National University, Daegu 41566, Korea

(Received 5 December 2014; Revised 1 July 2015; Accepted 11 August 2015)

ABSTRACT–The squeal noise occurring from the disc brakes of passenger cars has been analyzed by using the complex eigenvalue method numerically. The contact between a disc and two pads was analytically modeled as many linear springs and dampers in an effort to develop the improved equation of motion derived on the basis of Lagrange's equation and the assumed mode method. The finite element modal analysis results for disc brake components constitute an eigenvalue matrix in the analytical equation of motion. The complex eigenvalue analyses based on the equations of motion are able to examine the dynamic instability of a brake system, which is an onset of squeal, by considering the disc rotational effect. Numerical analyses showed that the modes unstable in an undamped analysis became stable in a damped case, which illustrates the important effect of damping on the squeal instability in a brake squeal simulation. Then several modified brake models were suggested and investigated how effectively they suppressed the occurrence of squeal noise. The brake parts such as a pad chamfer and a disc vane were modified and the influence of pad chamfer and vane shapes on squeal occurrence was proved to be significant. The numerical results showed that proper structural modification of a disc brake system can suppress the brake squeal to some extent.

KEY WORDS : Squeal, Complex eigenvalue analysis, Disc brake, Pad and vane, Damping, Finite elements

1. INTRODUCTION

The disc brake and its actuation system developed in the mid-1890s and first patented by the British engineer Lanchester (1902) have been advanced continuously. Brake squeal is commonly defined as the high-frequency noise above 1 kHz during brake engagement (Kinkaid and O'Reilly, 2003). The rising demand for automobile quietness and comfortableness has led researchers to study, predict and eliminate the brake squeal noise. Major efforts have been driven to the development of accurate mathematical models and efficient prediction methods for the squeal noise of disc brake systems (Ouyang *et al*., 2005).

Researchers recognize that friction forces are changeable by the change not only in friction coefficients but also in normal contacting forces due to vibration mode coupling. Even if a coefficient of friction is constant, friction force can still change and be sufficient to cause instability of a disc system. In terms of mathematics, the mode coupling leads to a non-symmetric stiffness coupling matrix in the equation of motion in contrast to the common symmetric coupling due to structural stiffness. Under some specific conditions in such a non-symmetric system, a pair of natural frequencies may merge and then become complex with further variations in the parameters of a disc system. The mode coupling phenomena can, therefore, be a fundamental mechanism for the onset of disc brake squeal. The occurrence of large oscillation due to mode coupling can be predicted by using the linear analysis of the models represented in two or more degrees of freedom.

North (1976) investigated for the first time the occurrence of brake squeal based on a constant friction coefficient and found out that brake squeal occurred as a result of self-excited vibration induced by friction forces. In previous research, disc brake systems have been commonly represented as minimal models (Shin *et al*., 2002, 2004; Flint and Hulten, 2002; von Wagner *et al*., 2007) or refined finite element models (Kung *et al*., 2000; Nack, 2000; Guan and Jiang, 1998) with large numbers of dof's. Even though the minimal model could easily be associated with an automotive disc brake and show basic characteristics of disc brake squeal, it has a limit in the representation of geometric shapes and modal behaviors accurately. The development of a comprehensive analysis method for the occurrence of disc brake squeal is still an unsolved issue that appears crucial from the perspective of brake manufacturers (Cantoni *et al*., 2009). Recently, Kang (2009) developed the finite element model of a rotating disc brake in a comprehensive manner. It showed that the stability characteristics of squeal noise was influenced by mode-coupling, gyroscopic effect and negative slope effect, and provided a good theoretical background in the

**Corresponding author.* e-mail: kimchul@knu.ac.kr

mechanism of the squeal phenomena.

Brake noise can be categorized to several classes based on either occurring frequencies or sources of excitations (Cantoni *et al*., 2009). Dai and Lim (2008) classified the brake noise into three categories depending on a frequency range, namely low-frequency noise (0 kHz ~ 1 kHz), low-frequency squeal noise (1 kHz ~ 3 kHz), and high-frequency squeal noise (3 kHz ~ 15 kHz). The low-frequency range can also be divided into three types in details – judder (0 kHz ~ 0.1 kHz), groan (0.1 kHz ~ 0.5 kHz) and its associated airborne noise called moan (0.1 kHz ~ 0.5 kHz), and howl (0.5 kHz ~ 1 kHz). The low-frequency squeal is generally classified as the noise with a narrow bandwidth in the frequency range above 1 kHz, while the high-frequency brake squeal is typically classified as the noise generated at frequencies above 3 kHz.

Liles (1989) suggested a finite element disc brake model coupled with adjacent components such as a rotor, pads, and a caliper, instead of the usual lumped parameter model. The analytic results were compared with the modal test data of an actual brake system. Spring elements with uniform stiffness were used to connect adjacent contact nodes on both interfaces of the rotor and linings. The equations of motion of the system were transformed to an eigenvalue problem solved by a complex eigenvalue analysis. Others (Guan and Jiang, 1998; Gaun and Huang, 2003) proposed a similar disc brake model consisted of a disc, pads, a caliper and a mounting bracket. The asymmetric stiffness matrix was obtained from the friction coupling between the disc and the pad. From the complex eigenvalue analysis, it was found that the brake system stability was greatly influenced by one mode of a disc and two modes of a mounting bracket, that were considered as key modes to be modified in order to suppress the brake squeal. However, how to effectively suppress the brake squeal by design changes was not proposed. Lee (2000) tried to optimize the complex eigenvalues of brake components on the basis of the QZ algorithm with MATLAB. Kang (2009, 2010) and Kang *et al*. (2008, 2009a, 2009b) proposed a mathematic model of a disc brake and showed the stability characteristics were influenced by mode-coupling, gyroscopic and negative slope effects. Mohammed and Rahim (2013) reviewed experiments and analyses on the disc brake squeal.

In most of previous analytic models for friction-coupled disc brakes had not been considered the damping of pad lining materials that was important for accuracy nor suggested necessary design changes for minimum squeal. In this study, an improved friction-coupled analysis method by considering the damping of a pad lining material is suggested. It enables us to examine the influence of the damping of friction materials on the occurrence of squeal and prevent from the over-prediction commonly seen in many squeal analyses. Several design changes in a disc brake are presented on the basis of the suggested method and their effects on squeal are examined. Natural frequencies and mode shapes of a disc and a pad are calculated from FE analysis and supplied for the equations of motion (EOM). EOM is solved by MATLAB.

2. MODELING AND FORMULATION

2.1. Analytical Model

The analytical model of a disc brake system is constructed as in Figure 1 to investigate the mode-coupled instability phenomena between a rotating disc and two brake pads with frictional linings in steady-sliding motion. The frictional lining on the pad is modeled as contact stiffness (k_C) and viscous damping (c_{lin}) that are assumed to be linear. One end (point P) of a pair of spring and damper is fixed to the pad surface and the other end (point D) is in contact with the disc.

It is assumed that the pad is loaded and kept under uniform pressure by a caliper. As the disc rotates in a constant angular velocity (Ω), frictional force is generated over the contact interfaces with two stationary pads loaded by a braking normal force (N_0). The contact forces are defined as in the global contact model (Heilig and Wauer, 2003). The contact surface is assumed to be undeformable and the centrifugal force is neglected due to slow speed while braking applies.

2.2. Contact Kinematics

Displacements of each point on a disc and two pads can be expressed in a cylindrical coordinate and unit vectors as in Figure 2, respectively, for dynamic analyses.

$$\vec{\mathbf{u}}^{tp}(r,\theta,z,t) = u^{tp}(r,\theta,z,t)\vec{e_r} + v^{tp}(r,\theta,z,t)\vec{e_\theta} + w^{tp}(r,\theta,z,t)\vec{e_z} \tag{1}$$

$$\vec{\mathbf{u}}^{D}(r,\psi,z,t) = u^{D}(r,\psi,z,t)\vec{e_r} + v^{D}(r,\psi,z,t)\vec{e_\theta} + w^{D}(r,\psi,z,t)\vec{e_z} \tag{2}$$

where the superscripts, p and D, denote both top and bottom pads and a disc, respectively. The slip angular velocity Ω takes place right after braking. The rotational

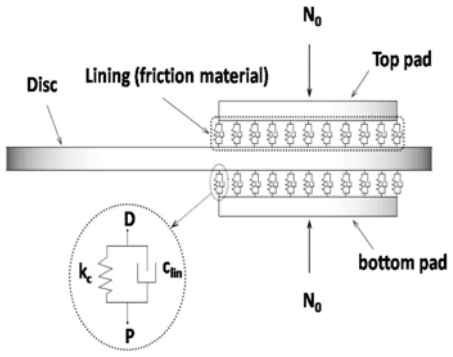

Figure 1. Schematics of a disc brake model used for analysis.

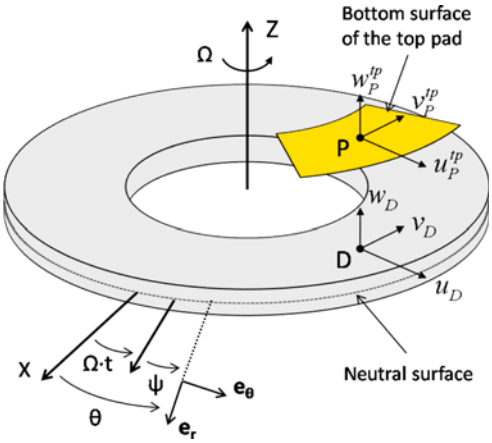

Figure 2. Reference (r, θ, z, t) and local (r, ψ, z, t) coordinates and contact displacements (u, v, w).

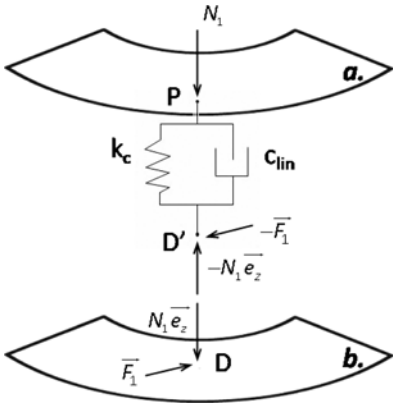

Figure 3. Contact force between (a) Bottom surface of a top pad; and (b) Contact area of a disc.

angles of a disc and a pad are θ and Ψ, respectively, after braking.

In Figure 3, contact forces (*i.e.*, brake and friction forces) are illustrated. Damping (c_{lin}) of a pad as well as stiffness are modelled and considered here, which was not included in the other work. A contact point D' on the friction material of the top pad at a point P is in contact with a point D on the disc, and it ends up with the expression as;

$$\vec{u}_{D'}^{tp}(r,\theta,t) = u_p^{tp}(r,\theta,t)\vec{e}_r + v_p^{tp}(r,\theta,t)\vec{e}_\theta + w_D(r,\theta,t)\vec{e}_z \tag{3}$$

The contact velocity vector at D' of the top pad is simply a partial time-derivative of Equation (3),

$$\vec{V}_{D'}^{tp} = \frac{\partial u_p^{tp}}{\partial t}\vec{e}_r + \frac{\partial v_p^{tp}}{\partial t}\vec{e}_\theta + \frac{\partial w_D}{\partial t}\vec{e}_Z \tag{4}$$

From the Coulomb's law of friction, which relates to kinetic friction (i.e., sliding friction) between moving surfaces, the contact frictional and normal forces are defined as;

$$\vec{F}_1 = -\mu \cdot N_1 (\vec{V}_{rel} / |\vec{V}_{rel}|) \tag{5}$$

$$N_1 = \frac{N_0}{A_c} + k_c(w_D - w_p^{tp}) + c_{lin}\frac{\partial(w_D - w_p^{tp})}{\partial t} \tag{6}$$

where the normal load N_1 is the sum of an initial brake pressure (N_0/A_c = force/contact area), spring and damping forces as in Figure 3. μ is a friction coefficient in Equation (A.9) and k_C is a spring rate and c_{lin} is a damping coefficient of a lining material. The relative velocity between pad and disc in Equation (5) can be expressed as;

$$\vec{V}_{rel} = \vec{V}_D - \vec{V}_D^{tp} \tag{7}$$

where the $\vec{V}_D$ is a contact velocity vector of the disc. Therefore, the term $\vec{V}_{rel} / |\vec{V}_{rel}|$ is a direction vector of the friction force at the contact surface. It can be linearized by the Taylor expansion at a steady sliding equilibrium such that (Kang, 2009);

$$\frac{\vec{V}_{rel}}{|\vec{V}_{rel}|} = \left\{\frac{1}{r\Omega}\left(\frac{\partial u_D}{\partial t} - \frac{\partial u_P^{tp}}{\partial t}\right) + \frac{1}{r}\left(\frac{\partial u_D}{\partial \theta} - v_D\right)\right\}\vec{e}_r + \vec{e}_\theta + \frac{1}{r}\frac{\partial w_D}{\partial \theta}\vec{e}_z + h.o.t \tag{8}$$

where r is a radius to the arbitrary point D and Ω represents an angular velocity of the disc as shown in Figure 2. The terms, $\frac{\partial u_D}{\partial \theta} - v_D$ and $\frac{\partial w_D}{\partial \theta}$ are associated with the frictional follower force (Ouyang and Mottershead, 2005) and neglected in subsequent formulation due to their insignificance (Kang *et al.*, 2009a, 2009b).

2.3. Equations of Motion

The equations of motion were derived on the basis of Lagrange equation by considering the pad friction. The transverse displacements of the disc and pad components are expressed in the modal expansion form to $N = (N_d + 2N_p)$ truncated modes by using an assumed mode method (Kang, 2009);

$$w^i(\vec{x},t) \cong \sum_{n=1}^{N} \varphi_{z,n}^i(\vec{x}) q_n^i(t), \quad \vec{q}^{\,i} = \left\{\vec{q}_1^{\,i}\, \vec{q}_2^{\,i} \cdots \vec{q}_N^{\,i}\right\} \tag{9}$$

where i is an upper pad, a lower pad and disc, and N is the numbers of the truncated modes of a disc and two pads, respectively. $\varphi_{z,n}^i(\vec{x})$ is the nth mode shape function obtained from the eigenfuctions of the top pad, disc and bottom pad components, respectively. Similarly, the tangential and radial displacements, (v^{tp}, v^{disc}, v^{bp}) and (u^{tp}, u^{disc}, u^{bp}) can be written in a similar fashion. The generalized coordinates are rearranged in a vector form as follows;

$$\{y\} = \{\vec{q}^{\,i}\} = \{y_1\ y_2 \cdots y_N\}^T \tag{10}$$

Based on the Lagrange method in the modal coordinate, the friction-coupled equations of motion can be derived as follows;

$$\frac{d}{dt}\left[\frac{\partial L}{\partial \dot{y}_m}\right]-\frac{\partial L}{\partial y_m}=\sum_{n=1}^{N} Q_{mn}(y_n), m, n=1,\cdots N \tag{11}$$

$$L=T-(U+U_c) \tag{12}$$

$$\delta W \equiv \sum_{m=1}^{N}\sum_{n=1}^{N} Q_{mn}(y_n)\delta y_m \tag{13}$$

where U_c is contact energy and U is total strain energy of a disc and two pads, and the total kinetic energy can be expressed as;

$$T=\sum T_i,\ \ i=tp,\ d,\ bp \tag{14}$$

$$T_i=\rho_i\int_{V_i}\left(\frac{\overrightarrow{d\mathbf{u}_i}}{dt}\cdot\frac{\overrightarrow{d\mathbf{u}_i}}{dt}\right)dV,\ \ i=tp,\ d,\ bp \tag{15}$$

where V_d and V_{tp}, V_{bp} are the volumes of a disc and two pads, respectively. The contact energy and the virtual work on both sides can be expressed as;

$$\begin{aligned} U_c &= U_{c.top}+U_{c,bottom} \\ &= \frac{k_c}{2}\int_{A_c}(w_D-w_p^{tp})^2\,dA+U_{c,bottom} \end{aligned} \tag{16}$$

$$\begin{aligned} \delta W &= \delta W_{top}+\delta W_{bottom} \\ &= \int_{A_c}\left\{(-\overline{N_1}-\overline{F_1})\cdot\delta\vec{u}_{D'}^{tp}+(\overline{N_1}+\overline{F_1})\cdot\delta\vec{u}_{D'}\right\}d+\delta W_{bottom} \end{aligned} \tag{17}$$

and the terms $U_{c,bottom}$ and δW_{bottom} on the bottom contact are skipped here, and similar to the top contact.

By the mass-normalization and linearization from Equation (11), the modified equations of motion which take a N × N matrix can be expressed as follows;

$$\{\ddot{y}\}+([C_{lin}]+[D]+[C_g])\{\dot{y}\}+([K_S]+[K_{ns}])\{y\}=\{0\} \tag{18}$$

where the detailed matrices are described in Equations (19) and (20) and Equations (A.1) ~ (A.6) in Appendix.

$$[D]=[C]+[C_{rd}]+[C_{ns}] \tag{19}$$

$$[K_S]=[\omega^2]+[K_C] \tag{20}$$

where $[C_{lin}]$ is the damping matrix of lining material, $[C]=diag(2\zeta_n\omega_n)$ is the structural damping matrix, $[C_{rd}]$ is the radial energy dissipative matrix originating from $\frac{1}{r\Omega}\left(\frac{\partial u_D}{\partial t}-\frac{\partial u_p^{tp}}{\partial t}\right)$ in Equation (8), $[C_{ns}]$ is the negative slope effect matrix associated with the negative slope of the variation of friction coefficient, $[C_g]$ denotes the gyroscopic effect matrix related to the damping effect from rotation of a disc, $[\omega^2]=diag(\omega_n^2)$ is the natural frequency matrix of system components, $[C_g]$ is the contact stiffness matrix, and the non-symmetric stiffness matrix, $[K_{ns}]$, is the non-conservative work matrix arising from friction coupling between a disc and two pads.

2.4. FEM Modal Anlysis

Referring to Appendix and Table 1, the values of parameters and data required for the equations of motion (EOM) can be obtained. The items (1) ~ (8) in Table 1 can be defined by referring to operation conditions and intrinsic parameters of a specific disc brake system. The values of the parameters in (9) and (10) are extracted from the modal analysis for a disc and two pads by finite element analyses. To compute natural frequencies and mode shapes necessary for solving the analytical equations of motion, finite element models of components with proper geometry were first developed. The FE models of a disc and a pad are shown in Figure 4. As boundary conditions, all nodes at the inner radius of the disc were fixed and others were free. The disc and pads are uniformly meshed in a cylindrical coordinate with hexahedral elements and the meshes in the contact region between the disc and pad are set to be identical. The detailed material and geometric parameters of the disc brake system are shown in Tables 2 and 3.

The contact FE model between a disc and a brake pad was constructed by using springs and dampers as shown in Figure 1. Special attention was paid to the determination of coefficients of stiffness and damping which mainly depended on the area of adjacent elements sharing a common node. In the contact area with uniform meshes as in Figure 4, the coefficients of stiffness and damping at the edge of the contact area are set to be reduced to 1/2 values inside. Besides, in the spring and damper pair at the

Table 1. Definition of parameters in EOMs.

No	Symbol	Definition
(1)	N_0	Pre-normal load
(2)	Ω	Rotational speed of a disc
(3)	k_C	Contact stiffness
(4)	μ	Friction coefficient
(5)	ζ_n	Modal damping ratio
(6)	c_{lin}	Damping coefficient of lining
(7)	A_C	Contact area
(8)	V_d	Volume of a disc
(9)	ω_n	Circular natural frequency
(10)	$[\varphi]$	Mode shape (modal displacement)

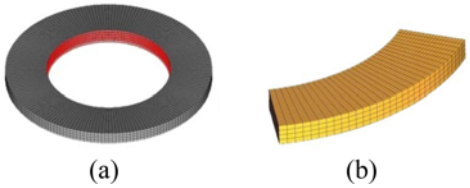

Figure 4. Finite element models: (a) Disc; (b) Pad.

Table 2. Dimensions of a disc and a pad.

Parameter	Value
Outer radius of a disc	152 mm
Inner radius of a disc	92 mm
Thickness of a disc	12 mm
Outer radius of a pad	144 mm
Inner radius of a pad	102 mm
Thickness of a pad	7 mm
Contact angle of a pad	64°

Table 3. Material properties of a disc and a pad.

Component	Density (ton/mm^3)	Young's modulus (MPa)	Poisson's ratio
Disc	7.1e-9	1.10e5	0.28
Pad	7.85e-9	2.07e5	0.30

corner of the interface, the values are reduced to 1/4 values inside. The normal forces in the spring and damper pair and the frictional forces at each contact node pair can be expressed in terms of component displacements at the contact nodes.

3. COMPLEX EIGENVALUE ANALYSES

3.1. Influence of Damping and Friction

In order to illustrate the mode-coupling phenomenon briefly and also to investigate the effect of the newly considered damping of a friction material on the occurrence of squeal, damped and undamped EOMs were considered. Then, the parametric studies on a frictional coefficient were performed on the basis of the complex eigenvalue analysis. The EOM in Equation (18) can be reduced to a following equation while neglecting pad damping,

$$\{\ddot{y}\}+([\omega^2]+[K_C]+[K_{ns}])\{y\}=\{0\} \quad (21)$$

The eigenvalue changes were investigated as the fiction coefficient, μ, varied from 0.0 to 0.7 and the unstable modes with different friction coefficients were identified from the complex eigenvalue analysis (CEA).

The influence of damping of lining material on squeal generation was investigated by using the damped EOM reduced from Equation (18) as follows;

$$\{\ddot{y}\}+[C_{lin}]\{\dot{y}\}+([\omega^2]+[K_C]+[K_{ns}])\{y\}=\{0\} \quad (22)$$

where $[C_{lin}]$ is a damping matrix. A constant damping coefficient of a lining material, 0.1 N·s/m, is used for following parametric studies.

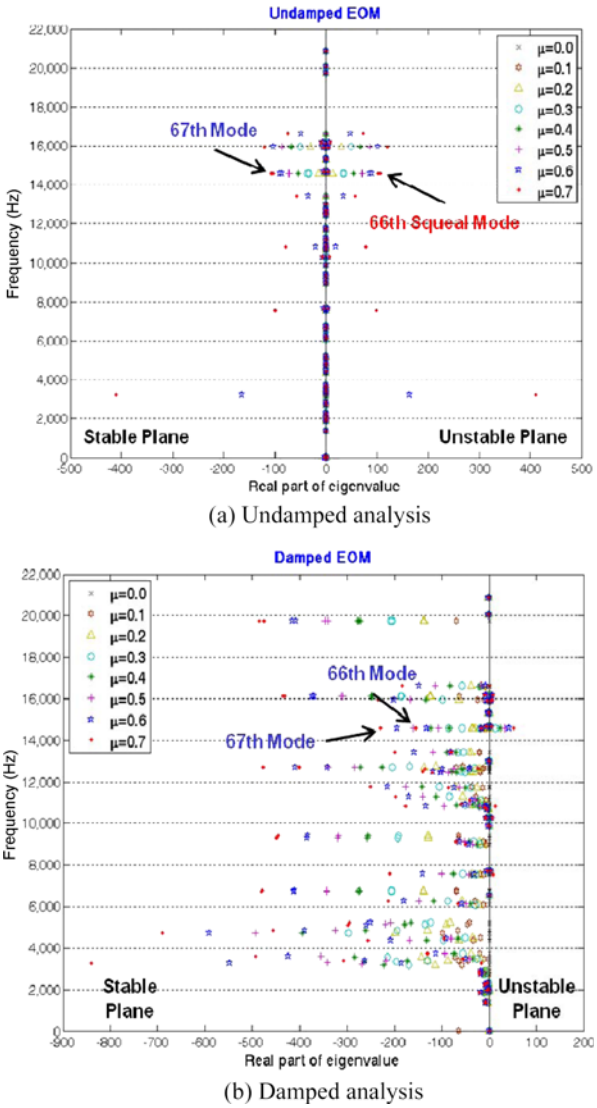

(a) Undamped analysis

(b) Damped analysis

Figure 5. Numerical results from the complex eigenvalue analyses with and without considering the pad damping effect of a lining material.

Figure 5 shows the numerical results from complex eigenvalue analyses for undamped and damped systems while the friction coefficient varies from 0.0 to 0.7. Let's focus on changes in the 66th and 67th modes. In the analysis of an undamped case, the 66th mode is an unstable mode and its adjacent mode, the 67th, lies in a stable region. In the analysis with damping, the 66th mode becomes stable. With increasing a friction coefficient from 0.25, the 66th mode in the undamped analysis is increasingly becoming unstable, as shown in Figure 6. However, the loci of the real part in the 66th mode remain in the stable region in the damped analysis.

As shown in Figure 7, the frequency loci of the 66th and 67th modes calculated from undamped complex eigenvalue analyses merge at the frictional coefficient

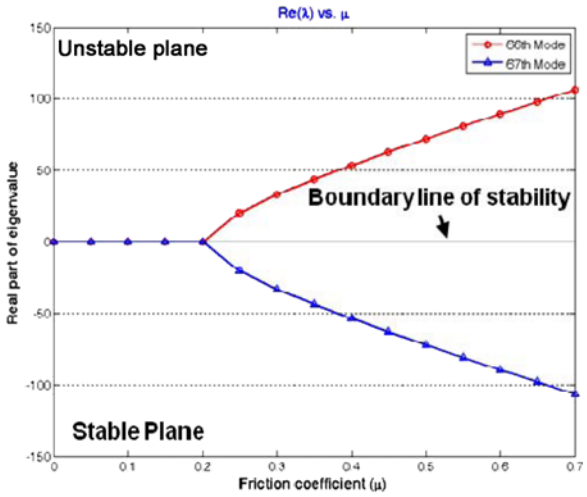

(a) Undamped analysis

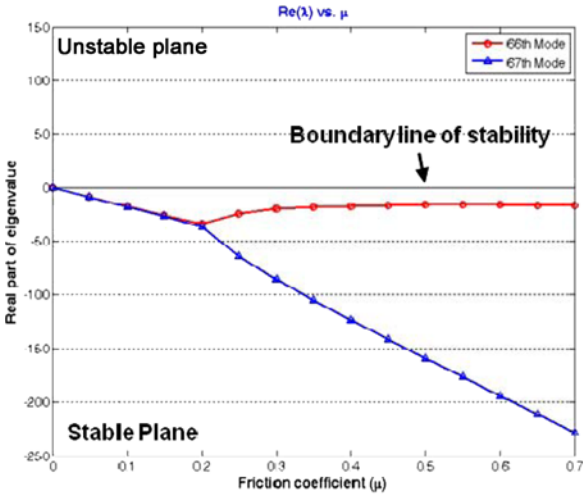

(b) Damped analysis

Figure 6. Stability variations in case of 66th and 67th modes depending on whether considering the pad damping or not.

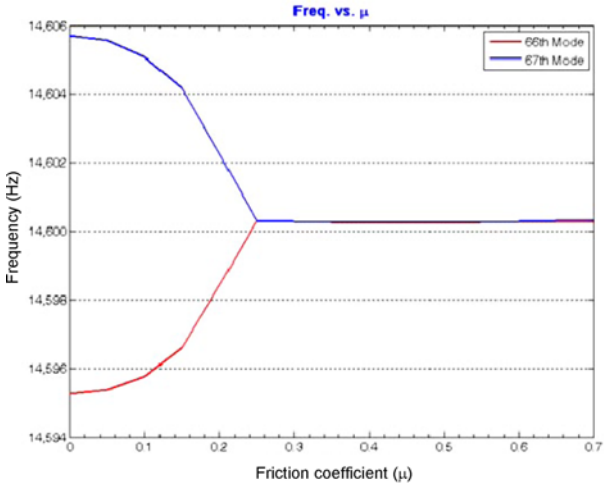

(a) Undamped analysis

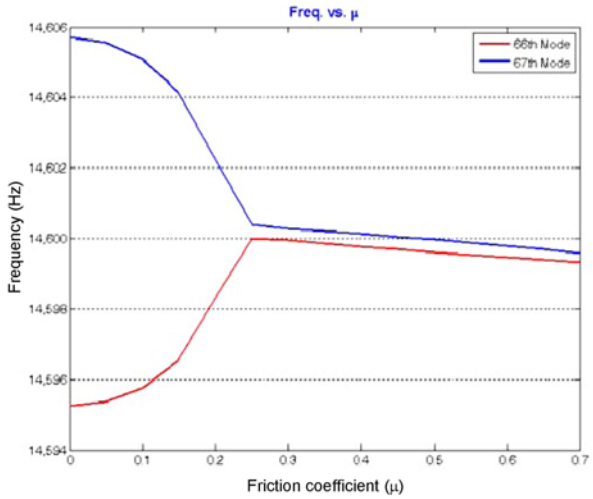

(b) Damped analysis

Figure 7. (a) Squeal occurs as a result of two modes coupling without considering pad damping; (b) No squeal and no mergence occurs with considering pad damping.

larger than 0.25. This demonstrates that the squeal occurs as a result of modes coupling. However, in analyses considering damping as in Figure 7 (b), the frequency loci of the 66th and 67th converge but never meet. As shown in Figure 5 (b), the 66th mode is stable (i.e., no squeal) in the analysis with damping, so that two modes does not merge. This result shows that the analysis considering damping is more realistic and accurate for the prediction of squeal.

Table 4 shows that the number of unstable modes reduces in the damped analyses. The results in the table confirm that the damping effect must be considered in squeal analyses.

Table 4. Number of unstable modes with undamped and damped analyses.

Frictional coefficient (μ)		0.1	0.2	0.3	0.4	0.5	0.6	0.7
No. of unstable modes	Undamped	7	8	10	10	13	15	15
	Damped	5	6	7	7	7	8	9

3.2. Squeal Suppression by Design Modification

How some design modifications of brake parts are effective in suppressing squeal occurrence is investigated in this section. The targeted brake parts to be modified are a pad chamfer and a disc vane. Figure 8 shows the 3-D brake model with a vented disc and two pads used in the study and the material properties of the disc brake system are summarized in Table 5.

Table 5. Material properties of a disc brake assembly.

Parts	Density (Ton/mm^3)	Young's modulus (MPa)	Poisson's ratio
Disc	7.05e-9	1.15e5	0.28
Pad	7.85e-9	2.07e5	0.29
Lining	2.60e-9	0.031e5	0.30

3.3. Modified Pad Chamfer Shape

The configuration of a brake pad chamfer determines the actual contact radius and the contact angle between a disc and a pad lining. Therefore, it may change the natural frequency and mode shape of a pad. The influence of a pad chamfer shape on squeal occurrence may be significant. Figure 9 shows a typical brake pad with chamfers. In order to investigate the influence of different chamfer patterns of lining on the occurrence of squeal noise, case studies have been performed. Uniform interface pressure of 500 kPa (5 bar) was applied for the four cases of pad champers. Therefore, the normal force, N_o in Equation (6), was adjusted to maintain braking pressure constant, as a contact area changed with the chamfer patterns as in Figure 10.

After FEM modal and complex eigenvalue analyses, the squeal mode in each case is identified. Figure 11 shows the real part results (i.e., unstable) from the complex eigenvalue analyses for the disc system in each case. The smaller a value of real eigenvalue is, the less the squeal occurs. The modified chamfer model gives the better squeal performance than the baseline one. The radial chamfer is likely to be the best in squeal suppression. Table 6 shows the occurrence of squeal modes at various frequencies in each model. The analysis model with a radial chamfer generated only a squeal mode at 6,875 Hz. The pad models with modified chamfers scarcely generated squeal at the low frequency below 6.8 kHz. The influence of design changes in a champer on squeal occurrence has been also verified very recently by dynamometer tests for passenger car squeal research from Tsinghua University. According to the experimental report, the squeal characteristics of the disc brake pad without champers were compared with those of the pad with champers by dynamometer tests. They reported that the maximum sound pressure level of the pad with champers was significantly lower than that without champers and the number of the squeal occurrence frequencies were

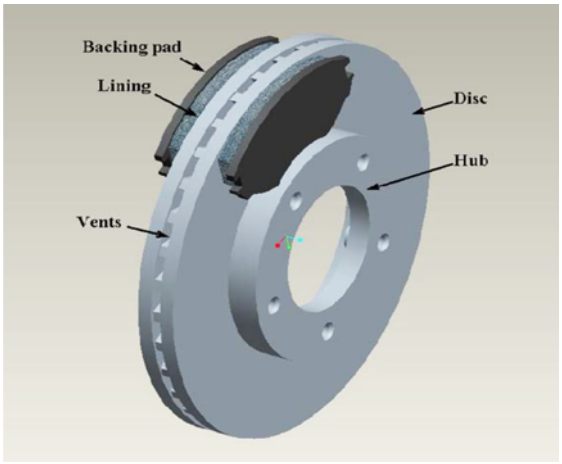

Figure 8. 3-D model of a disc brake assembly.

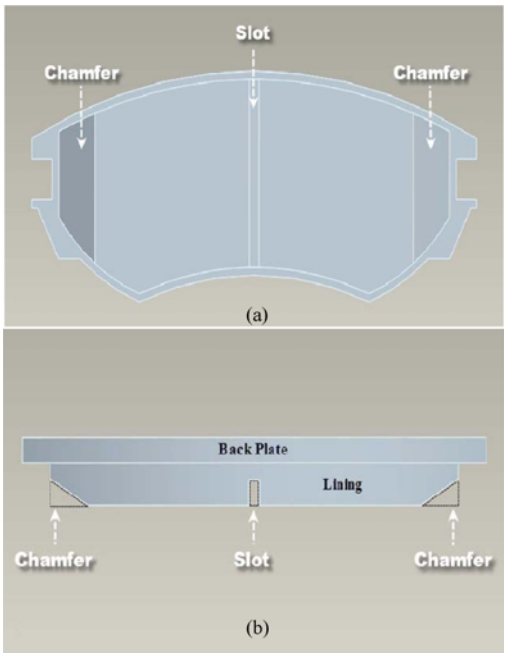

Figure 9. Typical brake pad with chamfers and a slot: (a) Front view; (b) Side view, and chamfers and a slot with removed material portions.

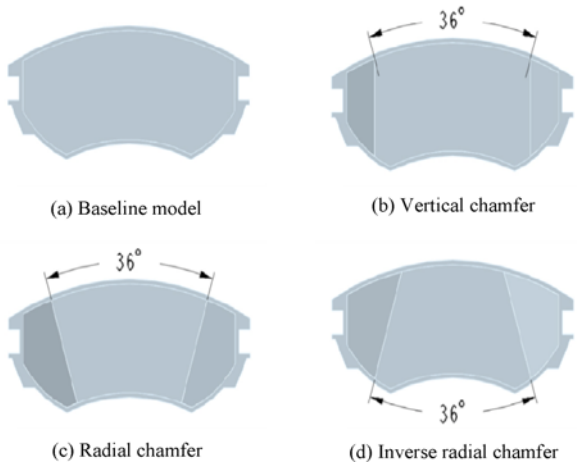

Figure 10. Baseline shape and the other three shapes of the pad chamfer.

markedly reduced by adding champers. Therefore, the numerical squeal results for the champer calculated from the currently proposed method can be validated to some extent.

In the baseline model, there are six squeal modes existed. The other three kinds of modified chamfers show less squeal modes than the baseline model. Two large squeal modes below 3 kHz in the baseline model were suppressed in all modified chamfered cases. The case of the inverse radial chamfer produces very small eigenvalues and the new 8th squeal mode that not exists in the original baseline model, as shown in Figure 11. The small eigenvalue means low possibility of squeal occurrence. The different chamfer pattern has a different influence on the system stability and the radial chamfer shows the best performance. Only one squeal mode (the 33rd) appears.

3.4. Modified Disc Vane Shape

The shape of a disc vane has a large influence on the

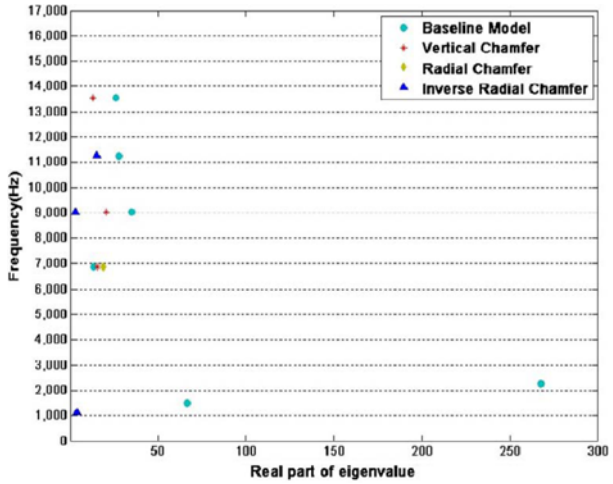

Figure 11. Squeal modes at complex eigenvalues in each chamfer model.

Table 6. Number of squeal modes at various frequencies in each chamfer model.

Squeal modes	Baseline model	Vertical chamfer	Radial chamfer	Inverse radial chamfer
8th (1,136 Hz)	×	×	×	○
10th (1,496 Hz)	○	×	×	×
16th (2,276 Hz)	○	×	×	×
33rd (6,875 Hz)	○	○	○	×
47th (9,040 Hz)	○	○	×	○
55th (11,251 Hz)	○	×	×	○
68th (13,555 Hz)	○	○	×	×
Total	6	3	1	3

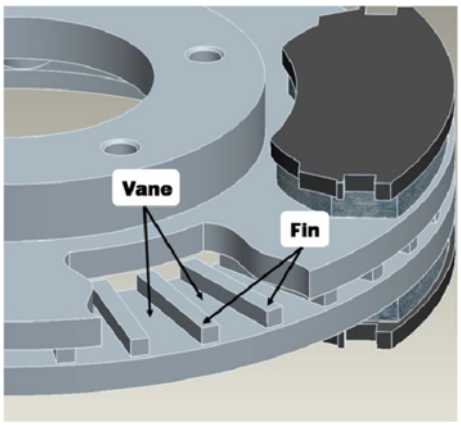

Figure 12. Typical configuration of disc vane.

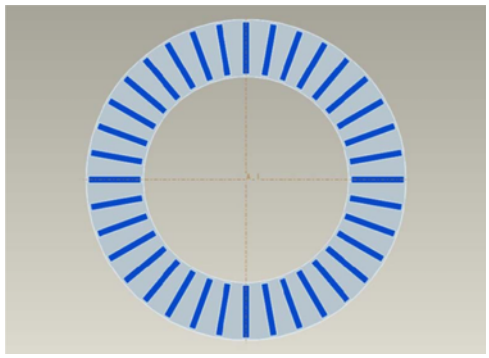

Figure 13. Baseline vane model for case studies.

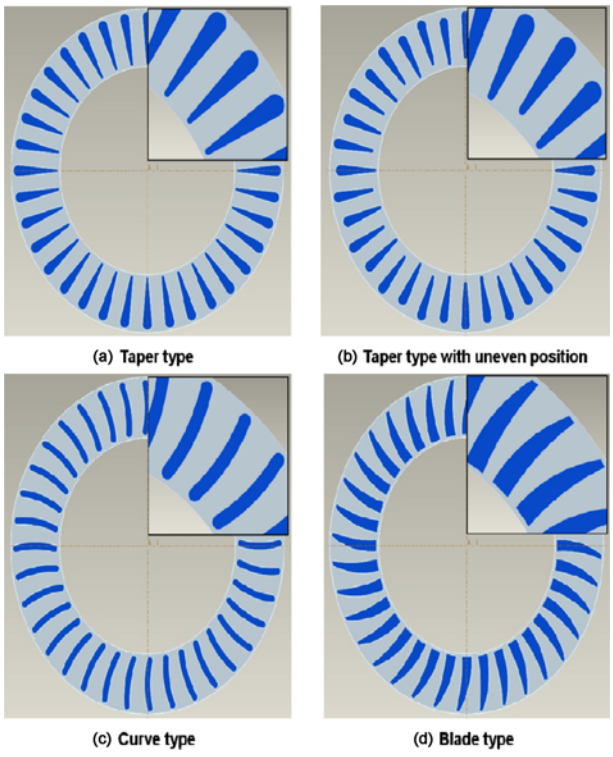

Figure 14. Configurations of disc vanes for case studies.

stability of a disc brake system because it changes the modal characteristics - mode shape and natural frequency. The degree of squeal generation was investigated, depending on various shapes of disc vanes. A configuration of a vane and a fin in a disc is shown in Figure 12. Five types of vane shapes are suggested and the baseline vane model is in a simple straight shape as shown in Figure 13. Other 4 configurations of the disc vane are depicted in Figure 14.

After modal and complex eigenvalue analyses, the squeal mode in each case was identified. Figure 15 represents the complex eigenvalues of various squeal modes in each case. Whether the squeal mode occurs or not at a different frequency in each case is summarized in Table 7. Again, the x-axis means an unstable real part and the y-axis stems from a imaginary part.

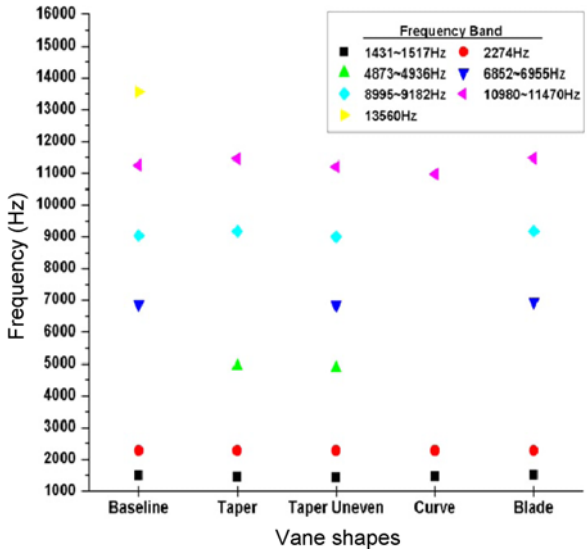

Figure 15. Squeal modes in the 5 cases in terms of their frequency bands.

Table 7. Occurrence of squeal modes in different frequencies band.

Squeal modes	Baseline	Taper	Taper uneven	Curve	Blade
1,431 Hz ~ 1,517 Hz	○	○	○	○	○
2,274 Hz	○	○	○	○	○
4,873 Hz ~ 4,936 Hz	×	○	○	×	×
6,852 Hz ~ 6,955 Hz	○	×	○	×	○
8,995 Hz ~ 9,182 Hz	○	○	○	×	○
10,980 Hz ~ 11,470 Hz	○	○	○	○	○
13,560 Hz	○	×	×	×	×
Total	6	5	6	3	5

* ○: Exist, ×: Not exist (suppressed)

In the baseline model there are six squeal modes. Different vane shape makes a different influence on the system stability. The squeal mode occurred in the baseline model at the frequency of 13,560 Hz disappeared in other 4 cases. The two squeal modes in the baseline model with the frequency under 3 kHz still exist in others 4 cases. The curve-type vane shape shows the best performance on the suppression of squeal because there are only 3 squeal modes.

4. CONCLUSION

A modified method to combine vibrational analytic equations and FEM considering an improved contact kinematics with pad damping is suggested for analyzing squeal of caliper disc brakes. The numerical results from CEA show that the analysis considering pad damping in EOM is more realistic and accurate for the prediction of brake squeal. Several design modifications of a disc and pads were carefully devised and their effectiveness to suppress squeal modes was investigated by using the proposed method.

(1) Damping of friction material can stabilize disc vibration and reduce the squeal.
(2) The modified pad chamfers gives better squeal characteristics than the baseline model (BM). The radial chamfer is likely to be best in squeal suppression. The 6 squeal modes existing in the BM pad was reduced to 1 or 3 squeal modes in the modified chamfers.
(3) The modified vane shapes cause a different influence on the squeal. The squeal mode occurred in BM at 13.56 kHz disappeared in other cases. The two squeal modes in BM at frequencies under 3.0 kHz still exist in other cases. The curved vane shows the best performance for suppression of squeal because only 3 squeal modes are left.
(4) It is noticeable that appropriate design changes of a disc vane and a pad show a large influence on the suppression of high frequency squeals.

REFERENCES

Cantoni, C., Cesarini, R., Mastinu, G., Rocca, G. and Sicigliano, R. (2009). Brake comfort – A review. *Vehicle System Dynamics* **47**, **8**, 901–947.

Dai, Y. and Lim, T. C. (2008). Suppression of brake squeal noise applying finite element brake and pad model enhanced by spectral-based assurance criteria. *Applied Acoustics* **69**, **3**, 196–214.

Flint, J. and Hulten, J. (2002). Lining-deformation-induced modal coupling as squeal generator in a distributed

parameter disc brake model. *J. Sound and Vibration* **254**, **1**, 1–21.

Guan, D. H. and Jiang, D. Y. (1998). A study on disc brake squeal using finite element methods. *SAE Paper No*. 980597.

Guan, D. and Huang, J. (2003). The method of feed-in energy on disc brake squeal. *J. Sound and Vibration* **261**, **2**, 297–307.

Heilig, J. and Wauer, J. (2003). Stability of a nonlinear brake system at high operating speeds. *Nonlinear Dynamics* **34**, **3-4**, 235–247.

Kang, J. (2010). Mode shape variation of disc brake with respect to contact stiffness variation. *Trans. Korean Society of Automotive Engineers* **18**, **3**, 127–132.

Kang, J., Krousgrill, C. M. and Sadeghi, F. (2008). Dynamic instability of a thin circular plate with friction interface and its application to disc brake squeal. *J. Sound and Vibration* **316**, **1-5**, 164–179.

Kang, J., Krousgrill, C. M. and Sadeghi, F. (2009a). Comprehensive stability analysis of disc brake vibrations including gyroscopic, negative friction slope and mode-coupling mechanisms. *J. Sound and Vibration* **324**, **1-2**, 387–407.

Kang, J., Krousgrill, C. M. and Sadeghi, F. (2009b). Analytical formulation of mode-coupling instability in disc-pad coupled system. *Int. J. Mechanical Sciences* **51**, **1**, 52–63.

Kang, J. Y. (2009). Squeal analysis of gyroscopic disc brake system based on finite element method. *Int. J. Mechanical Sciences* **51**, **4**, 284–294.

Kinkaid, N. M. and O'Reilly, O. M. (2003). Automotive disc brake squeal. *J. Sound and Vibration* **267**, **1**, 105–166.

Kung, S., Dunlap, K. B. and Ballinger, R. S. (2000). Complex eigenvalue analysis for reducing low frequency brake squeal. *SAE Paper No*. 2000-01-0444.

Lanchester, F. W. (1902). Improvements in the Brake Mechanism of Power-propelled Road Vehicles. G.B. Patent No. 26407.

Lee, H. W. (2000). *An Optimal Design Method for Brake Squeal Noise based on Complex Eigenvalue and Sensitivity Analyses and Response Surface Methodology.* Ph. D. Dissertation. University of Michigan. Ann Arbor, MI, USA.

Liles, G. D. (1989). Analysis of disc brake squeal using finite element methods. *SAE Paper No.* 891150.

Mohammed, A. Y. and Rahim, I. A. (2013). Analysing the disc brake squeal: Review and summary. *Int. J. Sci. Tech. Research* **2**, **4**, 60–72.

Nack, W. V. (2000) Brake squeal analysis by finite elements. *Int. J. Vehicle Design* **23**, **3/4**, 263–275.

North, M. R. (1976). Disc brake squeal. In: Braking of road vehicles. *Automobile Division of the Institution of Mechanical Engineers*, 169–176.

Ouyang, H., Nack, W., Yuan, Y. and Chen, F. (2005). Numerical analysis of automotive disc brake squeal: A review. *Int. J. Vehicle Noise and Vibration* **1**, **3/4**, 207–231.

Ouyang, H. and Mottershead, J. E. (2005). Dynamic instability of an elastic disk under the action of a rotating friction couple. *J. Applied Mechanics* **71**, **6**, 753–758.

Shin, K., Brennan, M. J., Joe, Y. G. and Oh, J. E. (2004). Analysis of disc brake noise using a two-degree-of-freedom model. *Int. J. Automotive Engineering* **5**, **1**, 61–67.

Shin, K., Brennan, M. J., Oh, J. E. and Harris, C. J. (2002). Analysis of disc brake noise using a two-degree-of-freedom model. *J. Sound and Vibration* **254**, **5**, 837–848.

von Wagner, U., Hochlenert, D. and Hagedorn, P. (2007). Minimal models for disk brake squeal. *J. Sound and Vibration* **302**, **3**, 527–539.

APPENDIX

Damping matrix of a lining frictional material;

$$[C_{\text{lin}}] = \mu c_{\text{lin}} \times \int_{A_C} \begin{bmatrix} [\varphi_\theta^{p1}]^T[\varphi_\theta^{p1}] & -[\varphi_\theta^{p1}]^T[\varphi_\theta] & [0] \\ -[\varphi_\theta]^T[\varphi_\theta^{p1}] & [\varphi_\theta]^T[\varphi_\theta^{p1}]\big|_t + [\varphi_\theta]^T[\varphi_\theta^{p1}]\big|_b & -[\varphi]^T[\varphi_\theta^{p1}] \\ [0] & -[\varphi_\theta^{p2}]^T[\varphi_\theta] & [\varphi_\theta^{p2}]^T[\varphi_\theta^{p2}] \end{bmatrix} dA \quad \text{(A.1)}$$

Radial dissipative matrix;

$$[C_{\text{rd}}] = \frac{p_0 \mu}{\Omega} \times \int_{A_C} \frac{1}{r} \begin{bmatrix} [\varphi_r^{p1}]^T[\varphi_r^{p1}] & -[\varphi_r^{p1}]^T[\varphi_r] & [0] \\ -[\varphi_r]^T[\varphi_r^{p1}] & [\varphi_r]^T[\varphi_r]\big|_t + [\varphi_r]^T[\varphi_r]\big|_b & -[\varphi_r]^T[\varphi_r^{p1}] \\ [0] & -[\varphi_r^{p2}]^T[\varphi_r] & [\varphi_r^{p2}]^T[\varphi_r^{p2}] \end{bmatrix} dA \quad \text{(A.2)}$$

Gyroscopic matrix;

$$[C_g] = \Omega\rho \times \int_{V_d} \begin{Bmatrix} [\varphi_r]^T\left(\left[\frac{\partial \varphi_r}{\partial \theta}\right] - [\varphi_\theta]\right) - \left(\left[\frac{\partial \varphi_r}{\partial \theta}\right] - [\varphi_\theta]\right)^T [\varphi_\theta] \\ + [\varphi_\theta]^T\left(\left[\frac{\partial \varphi_r}{\partial \theta}\right] - [\varphi_\theta]\right) - \left(\left[\frac{\partial \varphi_r}{\partial \theta}\right] - [\varphi_\theta]\right)^T [\varphi_\theta] \\ + [\varphi_Z]^T\left[\frac{\partial \varphi_Z}{\partial \theta}\right] - \left[\frac{\partial \varphi_Z}{\partial \theta}\right]^T [\varphi_Z] \end{Bmatrix} \begin{bmatrix} [0] & [0] & [0] \\ [0] & [1] & [0] \\ [0] & [0] & [0] \end{bmatrix} dV \quad \text{(A.3)}$$

Negative friction-slope effect matrix;

$$[C_{\text{ns}}] = p_0 \mu_{\dot{V}} \times \int_{A_C} \begin{bmatrix} [\varphi_\theta^{p1}]^T[\varphi_\theta^{p1}] & -[\varphi_\theta^{p1}]^T[\varphi_\theta] & [0] \\ -[\varphi_\theta]^T[\varphi_\theta^{p1}] & [\varphi_\theta]^T[\varphi_\theta]\big|_t + [\varphi_\theta]^T[\varphi_\theta]\big|_b & -[\varphi_\theta]^T[\varphi_\theta^{p1}] \\ [0] & -[\varphi_\theta^{p2}]^T[\varphi_\theta] & [\varphi_\theta^{p2}]^T[\varphi_\theta^{p2}] \end{bmatrix} dA \quad \text{(A.4)}$$

Contact stiffness matrix;

$$[K_C] = k_C \int_{A_C} \begin{bmatrix} [\varphi_Z^{p1}]^T[\varphi_Z^{p1}] & -[\varphi_Z^{p1}]^T[\varphi_Z] & [0] \\ -[\varphi_Z]^T[\varphi_Z^{p1}] & [\varphi_Z]^T[\varphi_Z]\big|_t + [\varphi_Z]^T[\varphi_Z]\big|_b & -[\varphi_Z]^T[\varphi_Z^{p1}] \\ [0] & -[\varphi_Z^{p2}]^T[\varphi_Z] & [\varphi_Z^{p2}]^T[\varphi_Z^{p2}] \end{bmatrix} dA \quad \text{(A.5)}$$

Non-symmetric non-conservative work matrix;

$$[K_{ns}] = \mu k_C \int_{A_C} \begin{bmatrix} [\varphi_\theta^{p1}]^T[\varphi_Z^{p1}] & -[\varphi_\theta^{p1}]^T[\varphi_Z] & [0] \\ -[\varphi_\theta]^T[\varphi_Z^{p1}] & [\varphi_\theta]^T[\varphi_Z]\big|_t + [\varphi_\theta]^T[\varphi_Z]\big|_b & -[\varphi_\theta]^T[\varphi_Z^{p1}] \\ [0] & -[\varphi_\theta^{p2}]^T[\varphi_Z] & [\varphi_\theta^{p2}]^T[\varphi_Z^{p2}] \end{bmatrix} dA \quad \text{(A.6)}$$

$$\mu(t) = \left\{ \mu_k + (\mu_s - \mu_k) e^{-\alpha|\bar{V}_{rel}|} \right\} \quad \text{(A.7)}$$

$$\mu_{\dot{V}} = -\alpha(\mu_S - \mu_K) e^{-\alpha\Omega r_{cer}} \quad \text{(A.8)}$$

where the subscripts t and b denote the top and bottom contact locations at z = h/2 and z = –h/2, respectively. $N_0/A_c = p_0$ is the initial pressure. The parameters, ζ_n and ω_n, denote the damping ratio and natural frequencies of the disc and pad components, and $\mu_{\dot{V}}$ in equations (A.4, A.8) represents the slope of a friction coefficient with respect to a sliding speed and μ_s and μ_k are static and kinetic friction coefficients, respectively, α is a control parameter, and r_{cer} is a centroid of a contact area (Kang, 2009).